

8 Element Strategy Initiative to Form Core Research Center for Electron Materials

– Multi-probe study using X-rays, muons and neutrons –

*Youichi Murakami, Hiroshi Kumigashira,
Kenji Kojima, Jun-ichi Yamaura*

8-1 Introduction

The national project “Elements strategy initiative to form core research center for electron materials” was started in 2012. We are aiming to develop entirely new materials that use ubiquitous elements, based on successful experience far away from development policy, and are pioneering electronic materials to create new guidelines for material design using harmless elements to open up new fields of material science. We are researching the crystal, local, electronic, and magnetic structures of new functional materials using synchrotron radiation, muon and neutron sources.

8-2 Complete structure determination of thin film superconductor $\text{Ba}_{1-x}\text{La}_x\text{Fe}_2\text{As}_2$

Epitaxial thin films are a good platform to study applications and functional materials. Epitaxial growth often produces additional structural distortion and atomic position displacements from the original ones in bulk crystals. Thus, the crystal structure of thin films is an important factor to understand the functionality of a material. Iron-based superconductors, a new family of high- T_c superconductors, have been studied since their discovery in 2008. Recently, there has been growing interest in the thin films of iron-based

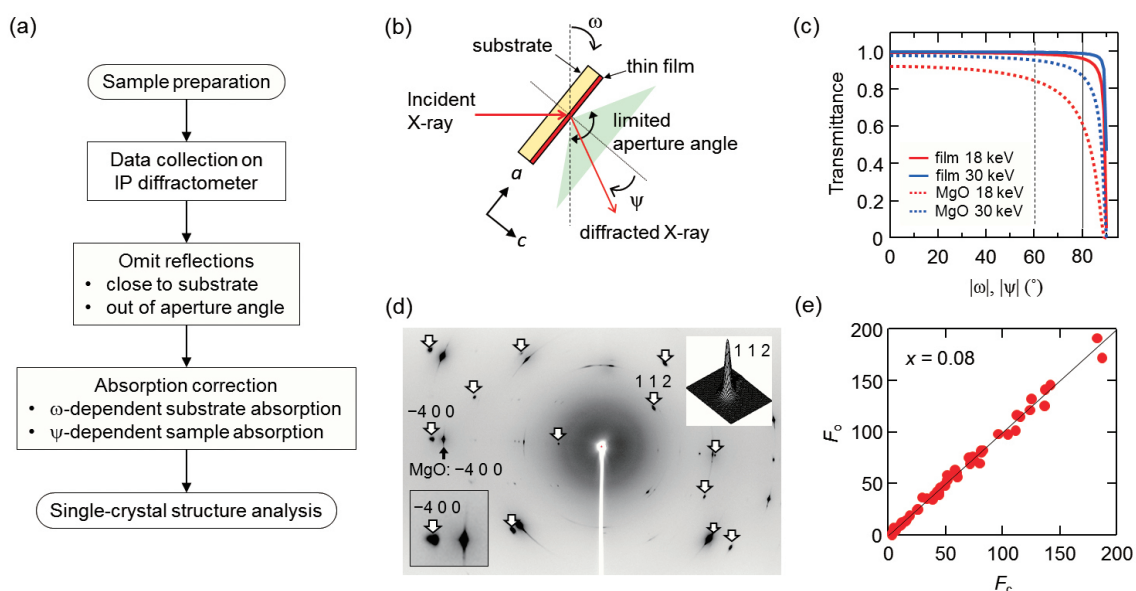


Fig. 1: (a) Flowchart outlining single-crystal thin-film structure analysis. (b) Schematic of the X-ray diffraction experiment. (c) ω - and ψ -dependence of X-ray transmittance for 200 nm $\text{Ba}_{1-x}\text{La}_x\text{Fe}_2\text{As}_2$ thin film and 0.1 mm MgO substrate at wavelengths of 0.68882 Å and 0.42032 Å. (d) Oscillation photograph of $\text{Ba}_{0.92}\text{La}_{0.08}\text{Fe}_2\text{As}_2$ thin film. The arrows indicate the reflections from the thin film. The left lower inset shows the $-4\ 0\ 0$ reflection, and the right upper inset shows the three-dimensional profile of the $1\ 1\ 2$ reflection. (e) Observed (F_o)–calculated (F_c) structure factors plotted for $x = 0.08$.

superconductors that exhibit high critical current density. The highest T_c achieved to date is for a FeSe monolayer on a SrTiO₃ substrate. A close relationship between T_c and $FePn_4$ geometry (Pn = pnictogen) has been proposed for this family; thus, their detailed crystal structures need to be identified to understand their superconductivity mechanism.

Here, we demonstrate a procedure for crystal structure analysis of an epitaxial thin film using a synchrotron X-ray source and area detector. This film cannot be grown by solid-state reaction but can be deposited on a substrate. A flowchart of the method used for the structure analysis of the thin films is presented in Fig. 1(a) [1]. After the film was deposited on the MgO substrate with a thickness of 0.5 μm, the substrate was thinned to ~0.1 μm by a dicing saw. The incident X-ray beam passed through the substrate and the film was always located on the downstream side of the beam, as illustrated in Fig. 1(b). The intensities were omitted and corrected because of the strong absorption effect of the substrate and thin film for incident and diffracted beams. Figure 1(c) shows the transmittance of the substrate and film as a function of the angle between the incident X-ray and substrate ω , and the angle between the diffracted X-ray and film ψ , as defined in Fig. 1(b). Transmittance becomes extremely weak at high ω and ψ values. Thus, the total oscillation photographs were exposed within the range of $-60^\circ < \omega < +60^\circ$, and intensities over $|\psi| > 80^\circ$ were omitted. The main steps of this process are shaded in Fig. 1(a).

Figure 1(d) shows the oscillation photograph for Ba_{1-x}La_xFe₂As₂ with $x = 0.08$. The absorptions of the substrate and film were corrected using an in-house program. Atomic positions and anisotropic displacement parameters for all atoms were refined according to the full-matrix least-squares method using SHELXL. The structural models were based on a reported one of BaFe₂As₂ belonging to space group $I4/mmm$. Figure 1(e) plots the observed structure factors (F_o) as a function of the calculated structure factors (F_c) for $x = 0.08$, revealing that the structure is well refined.

The atomic positions in the film were determined with an accuracy of ± 0.005 Å. This method can now be applied to films with a lattice mismatch with the substrate larger than ~3%. An improved process for the integration of reflections will allow analysis of the structure of thinner films

and ones with smaller lattice mismatch.

8-3 Electron-hydroxyl state as electron donor in mayenite

Mayenite, Ca₁₂Al₁₄O₃₃ (C12A7), comprises a class of cage structured compounds that has been drawing much attention since they exhibit persistent photoconductivity upon hydrogenation and serve as an electrone, in which the electron behaves as an anion. Mayenite is composed of calcium oxide (12CaO) and alumina (7Al₂O₃), which is made of the first, third, and fifth elements in the order of the Clarke number (natural abundance of individual elements in the earth's crust), attracting broad interest in regard to "green technology" where the replacement of rare chemical elements with useful functionalities with such common materials is the central focus.

Here, we report on the electronic structure of a muon as pseudohydrogen in mayenite [Ca₂₄Al₂₈O₆₄]⁴⁺[2(1-x)O²⁻+4x(e⁻)], with three different levels of electron doping, namely, pristine ($x = 0$), 10^{19} cm⁻³, and 10^{21} cm⁻³ ($x \sim 1$), investigated using muon spin rotation (μ SR) spectroscopy. μ SR is a powerful technique for simulating the electronic structure of interstitial H. Figure 2(a) shows weak transverse field (wTF) and zero-field (ZF) μ SR time spectra for pristine (a), 10^{19} cm⁻³ (b), and 10^{21} cm⁻³ (c) samples [2]. All the wTF spectra exhibit damping oscillations with a frequency expected for the diamagnetic muon state (i.e., Mu⁺ or Mu⁻, Mu: muonium), $\omega = \gamma_\mu B_{\text{ext}}$, where γ_μ is the muon gyromagnetic ratio. While the spectra exhibit negligibly slow depolarization at 300 K, the depolarization rate is enhanced at 5 K, with a tendency of greater depolarization for a lower carrier concentration. As is confirmed in the ZF- μ SR spectra at 5 K (filled diamonds), the envelope function exhibits an exponential behavior, suggesting that depolarization is induced by an unpaired electron. It is also noticeable that the pristine and 10^{19} cm⁻³ samples exhibit a slight reduction of the initial polarization at low temperatures.

Based on the curve fit of the wTF- μ SR spectra as reported in literature [2], the depolarization rates due to nuclear magnetic moments δ_n are estimated at $\delta_n = 0.080, 0.055, 0.044$ μs⁻¹ for pristine, 10^{19} cm⁻³, and 10^{21} cm⁻³ samples, respectively. We also calculated δ_n by the dipole-fields at the muon site deduced from first-principles

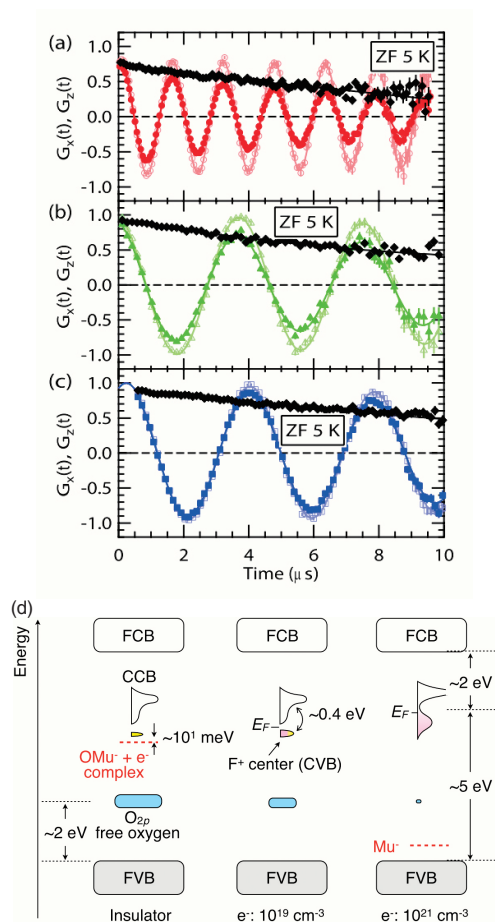


Fig. 2: (a) wTF- μ SR time spectra at 300 and 5 K in mayenite with (a) pristine (5 mT), (b) 10^{19} cm^{-3} (2 mT), and (c) 10^{21} cm^{-3} (2 mT) doping levels. ZF- μ SR spectra observed at 5 K are also shown by filled diamonds to confirm the line shape of the envelope function. (d) Schematic energy diagrams of mayenite. The blue (pink) and yellow hatched regions show the occupied levels of oxygen (electron) in the cage center. The red dashed lines show the electronic levels associated with muon. FCB (FVB) and CCB (CVB) denote the frame conduction (valence) band and cage conduction (valence) band, respectively.

calculation. The calculated values are in good agreement with the experimental values obtained; thus it is suggested that the muons implanted into the pristine sample are bound to oxygen at the cage center.

The high-field time spectra (not shown here) yields the high-precision frequency shift K_μ , estimated at $K_\mu = +0.3 \text{ ppm}$ (pristine) and $+6.6 \text{ ppm}$ (10^{21} cm^{-3}). These values coincide with the proton chemical shift in relevant compounds observed by $^1\text{H-NMR}$, i.e. -0.8 ppm in C12A7:OH^- and $+5.1 \text{ ppm}$ in C12A7:H^- . Thus, we can assign the chemical state of diamagnetic muon in the pristine and 10^{21} cm^{-3} samples to OMu^- and Mu^- , respectively.

The energetics of Mu/H in the band structure

of mayenite may be understood from the schematic diagrams shown in Fig. 2(d). The conduction band consists of the frame conduction band (FCB) and cage conduction band (CCB), where CCB is associated with electrons at the cage center. In pristine mayenite, CCB is unoccupied while free O^{2-} 2p levels form the occupied state located at 2 eV above the frame valence band (FVB). Slight electron doping divides the CCB to an empty band and fully occupied cage valence band (CVB, similar to the F^+ center observed in CaO) due to the polaron formation. By further electron doping, the kinetic energy gain surpasses the lattice distortion to induce the insulator-to-metal transition. Therefore, it is presumed that the OMu^- hydroxyl base in pristine mayenite serves as an electron donor to the vacant cage to form the F^+ -like center ($\{OMu^-e^-\} \rightarrow \{OMu^- \} + \{e^-\}$). Meanwhile, the electronic level associated with Mu^- in the 10^{21} cm^{-3} sample would be situated deep in the band gap, as is suggested from the photon energy ($h\nu \sim 4 \text{ eV}$) required for inducing the reaction $\{H^-\} + h\nu \rightarrow \{H^0 \} + \{e^-\}$. Considering that there still remain many vacant cages available for muons even in the 10^{21} cm^{-3} sample, the present result indicates that a muon (as well as H) is unstable as an isolated Mu^+ or Mu^0 in mayenite.

8-4 Interlayer “anionic electrons” states in honeycomb lattice based compounds $Ae\text{AlSi}$ ($Ae = \text{Ca, Sr, Ba}$)

Honeycomb lattice compounds have drawn considerable attention in the field of condensed matter physics in recent decades. In addition to a variety of quantum transport properties, many materials with related structures exhibit superconducting transitions with relatively high critical temperatures, e.g. MgB_2 , $Ae\text{AlSi}$ ($Ae = \text{Ca, Sr, Ba}$), and graphite-intercalated compounds. We report that the interlayer states common to the compounds $Ae\text{AlSi}$ ($Ae = \text{Ca, Sr, Ba}$) arise from F-center-like electrons arrayed in periodic cavities.

The $Ae\text{AlSi}$ compounds crystallize in the SrPtSb -type structure and can be viewed as metal-sandwiched variants of a honeycomb lattice (Fig. 3(a)) [3]. In this crystal, the large distance between layers leaves open significant interstitial spaces X, as depicted in Fig. 3(a). Geometrically, the site X is located in a trigonal bipyramidal Ae_3Al_2 cage with the fractional coordinates of $(2/3,$

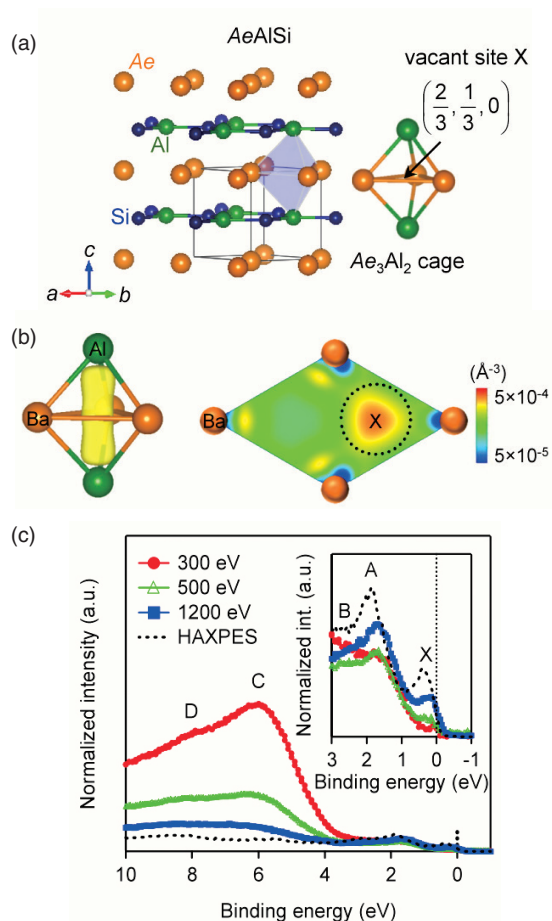


Fig. 3: (a) The crystal structure of AeAlSi ($Ae = Ca, Sr, Ba$). The Ae_3Al_2 cage is shown with a light blue polyhedron, and the vacant site X in the Ae_3Al_2 cage is indicated with a black arrow. (b) The electron density of BaAlSi (left) isolated in the Ba_3Al_2 cage shown with an isosurface of 4×10^{-4} electrons \AA^{-3} . The electron density map (right) projected onto the (0 0 1) face of BaAlSi. (c) The valence band SXPES spectra of BaAlSi. The energies of the incident X-rays used were $h\nu = 300, 500,$ and 1200 eV, respectively. The inset highlights the spectra with binding energy of $-1 < E_B < 3$ eV. The black dashed line represents corresponding HAXPES data measured with $h\nu \sim 6000$ eV.

$1/3, 0$).

From first-principles calculation, we can see an electron density peak on the vacant site X, suggesting the possibility of anionic electrons captured inside the cage as shown in Fig. 3(b).

The orbital character of the interlayer state can be confirmed by soft X-ray photoemission spectroscopy (SXPES). In Fig. 3(c), clear Fermi edges as well as characteristic peaks (X, A, B, C, and D) are observed. It is noteworthy that the normalized intensity of the peak X (anionic electrons) is enhanced with increasing $h\nu$, whereas the peak C (Al/Si $3p_{x,y}$ orbitals) is suppressed. These results

imply that the orbital character of peak X, which shows contrastive intensity modulation to the peak C, is different from Al/Si $3p$ orbitals, whereas it supports the F-center scenario. Note that the peaks A and B (Al/Si $3p_z$ orbitals) exhibit similar intensity modulation to X, since F-center and Al/Si $3p_z$ electrons exhibit significant orbital hybridization. These data are fully consistent with the anionic electron state obtained from the electronic state calculation.

References

- [1] Structure determination in thin film $Ba_{1-x}La_xFe_2As_2$: relation between $FeAs_4$ shape and superconductivity, K. Kobayashi, A. Nakao, S. Maki, J. Yamaura, T. Katase, H. Sato, H. Sagayama, R. Kumai, Y. Kuramoto, Y. Murakami, H. Hiramatsu, and H. Hosono, submitted to Phys. Rev. B.
- [2] Cage electron-hydroxyl complex state as electron donor in mayenite, M. Hiraishi, K. M. Kojima, M. Miyazaki, I. Yamauchi, H. Okabe, A. Koda, R. Kadono, S. Matsuishi, and H. Hosono, Phys. Rev. B **93**, 121201(R) (2016).
- [3] Interlayer states arising from anionic electrons in the honeycomb-lattice-based compounds AeAlSi ($Ae = Ca, Sr, Ba$) Y. Lu, T. Tada, Y. Toda, S. Ueda, J. Wu, J. Li, K. Horiba, H. Kumigashira, Y. Zhang, and H. Hosono, Phys. Rev. B **95**, 125117 (2017).